International Forum on Aeroelasticity and Structural Dynamics
IFASD 2019
9-13 June 2019, Savannah, Georgia, USA

DESIGN OF STABILITY AUGMENTATION SYSTEMS FOR FLEXIBLE AIRCRAFT USING PROJECTIVE CONTROL

Rafael M. Bertolin[1], Antônio B. Guimarães Neto[1], Guilherme C. Barbosa[1], Juliano A. Paulino[1], Flávio J. Silvestre[2]

[1]Instituto Tecnológico de Aeronáutica
São José dos Campos, São Paulo, Brasil
rafaelmbufsj@gmail.com
antonio@ita.br
guichavesbarbosa@gmail.com
juliano@gmail.com

[2]Technische Universität Berlin
Marchstrasse 12, 10587 Berlin, Germany
flavio.silvestre@tu-berlin.de

Keywords: SAS, flexible aircraft, projective control, X-HALE

Abstract: There are many challenges related to the design and operation of flexible aircraft. Flight control law design for improving handling qualities is one of them because the major problem in the design of controllers then concerns aeroservoelastic stability. To deal with this difficulty, methodologies for flight control law design considering the aeroelastic dynamics of the aircraft are being pursued. In this paper, an output-feedback-based stability augmentation system is proposed and designed to improve the handling qualities of a flexible aircraft and to increase the structural damping of some of its aeroelastic modes. The design is based on the projective control technique, which allows preserving in the closed-loop system the eigenstructure of certain modes of interest whose dynamic characteristics stem from an optimal state feedback solution. The X-HALE flexible aircraft is considered. Numerical studies by means of nonlinear simulations allow testing and confirming the effectiveness of the proposed controller.

1 INTRODUCTION

Flexible aircraft (FA) are characterized by low or very low frequencies of their aeroelastic modes and, as a consequence, strong, undesirable and even dangerous couplings between the aeroelastic and the rigid-body flight dynamics may occur. Active control systems play an important role in addressing these problems, especially after the development of fly-by-wire technologies. However, flight control law design for FA is still a very challenging task [1].

One of the major problems in the FA control law design process concerns aeroservoelastic (ASE) stability. Traditionally, the design is based on a rigid-body model with quasi-steady corrections, and ASE stability problems are solved afterward by the addition of low-pass or notch filters in the feedback and feedforward loops [2, 3]. However, with a tighter separation between the frequency ranges of the rigid-body and of the aeroelastic dynamics, this procedure can lead to low-performance controllers, degrade handling and ride qualities, be inadequate to filter elastic effects in the measured signals or even cause instabilities [3]. Therefore, methodologies for flight control law design taking into account the aeroelastic dynamics are being pursued [2, 3].

In this paper, the development of a robust projective controller [4, 5] designed using the dually-constrained axis formulation for the FA flight dynamics [6, 7] is proposed. It corresponds to an output-feedback-based stability augmentation system (SAS) to improve the flight dynamics characteristics and the structural damping of the FA X-HALE [8]. Numerical comparisons with an approach based on full state feedback theory [3] and evaluation by means of nonlinear simulations are also part of this work.

2 PROJECTIVE CONTROL OVERVIEW

Projective control is an output-feedback-based control approach able to retain a partial or the dominant eigenstructure of a closed-loop reference plant designed using state feedback control. The main goal is to preserve performance and robustness characteristics of the closed-loop reference dynamics employing static and/or dynamic output feedback [4, 5].

The projective control methodology combines optimal state feedback control with eigenstructure assignment [4]. Eigensystem synthesis techniques are very practical and suitable for flight control systems because they easily allow incorporating frequency, damping and decoupling specifications in terms of desired closed-loop eigenvalues and eigenvectors [2]. Such methodology employed with a unified dynamic model comprising both structural and rigid-body degrees of freedom seems to be an attractive solution for the FA control problems. Furthermore, the use of output feedback in the control law makes the implementation more feasible and avoids problems arising from state feedback techniques based upon observer theories, such as controllers of high order and degradation of stability margins.

Consider the problem of designing output feedback regulators for a linear time-invariant (LTI) system described by:

$$\dot{\mathbf{x}} = \mathbf{A}\mathbf{x} + \mathbf{B}\mathbf{u} \tag{1}$$

$$\mathbf{y} = \mathbf{C}\mathbf{x} \tag{2}$$

where $\mathbf{x} \in \mathbb{R}^{n_x}$, $\mathbf{u} \in \mathbb{R}^{n_u}$ and $\mathbf{y} \in \mathbb{R}^{n_y}$ are the states, controls and measured outputs, respectively, and with minimal realization ($\mathbf{A}$, $\mathbf{B}$, $\mathbf{C}$).

Let the optimum state feedback solution be given by [9]:

$$\mathbf{u} = -\mathbf{R}^{-1}\mathbf{B}^{\mathbf{T}}\mathbf{P}\mathbf{x} = -\mathbf{K}_{\mathbf{x}}\mathbf{x} \tag{3}$$

with $\mathbf{P}$ being the unique symmetric positive-definite solution of the algebraic Riccati equation (ARE):

$$\mathbf{A}^{\mathbf{T}}\mathbf{P} + \mathbf{P}\mathbf{A} + \mathbf{Q} - \mathbf{P}\mathbf{B}\mathbf{R}^{-1}\mathbf{B}^{\mathbf{T}}\mathbf{P} = \mathbf{0} \tag{4}$$

where $\mathbf{Q} \geq 0$ and $\mathbf{R} > 0$ are symmetric matrices serving as design parameters.

The state feedback control law (Eq. (3)) results in a system with satisfactory closed-loop reference dynamics:

$$\dot{\mathbf{x}} = (\mathbf{A} - \mathbf{B}\mathbf{K}_{\mathbf{x}})\,\mathbf{x} = \mathbf{F}\mathbf{x} \tag{5}$$

characterized by its eigenvalues and associated invariant subspaces ($\mathbf{F}\mathbf{V} = \mathbf{V}\mathbf{\Lambda}$, where $\mathbf{\Lambda}$ and $\mathbf{V}$ are the eigenvalue and eigenvector matrices, respectively).

If there are n_y outputs available for feedback, as described by Eqs. (1) and (2), using the following control law:

$$\mathbf{u} = -\mathbf{K}_{\mathbf{y}}\mathbf{y} \tag{6}$$

then, n_y eigenvalues ($\mathbf{\Lambda}_{n_y}$) and their associated eigenvectors ($\mathbf{V}_{n_y}$) of the state feedback design can be retained using static output feedback gains given by [4]:

$$\mathbf{K_y} = \mathbf{K_x}\mathbf{V}_{n_y}\left(\mathbf{C}\mathbf{V}_{n_y}\right)^{-1} \tag{7}$$

where the eigenvectors $\mathbf{V}_{n_y}$ and eigenvalues $\mathbf{\Lambda}_{n_y}$ satisfy the following equation:

$$\mathbf{F}\mathbf{V}_{n_y} = \mathbf{V}_{n_y}\mathbf{\Lambda}_{n_y} \tag{8}$$

The control law given by Eqs. (6) and (7) and satisfying Eq. (8) corresponds to a projective control [5].

3 THE X-HALE AIRCRAFT

The X-HALE is an unmanned remotely-piloted experimental airplane originally developed by Professor Carlos Cesnik and coworkers at the University of Michigan (U-M)[1] to serve as a test platform to collect aeroelastic data coupled with the aircraft rigid-body motion, aiming to validate mathematical formulations of flexible aircraft flight dynamics and control system design techniques [8].

It is a wing-boom-tail type aircraft, with modular airframe that can be configured to fly as a four-meter-span (with wing aspect ratio $AR = 20$), six-meter-span ($AR = 30$) or eight-meter-span ($AR = 40$) configuration. In all of them, the outer wing panels are mounted with a 10-degree dihedral angle. The central tail can be flipped in flight to either a horizontal or a vertical position to significantly modify the lateral-directional stability of the aircraft. This work considers only the four-meter-span, vertical-central-tail configuration, shown in Fig. 1.

Figure 1: Four-meter-span, vertical-central-tail X-HALE configuration.

Recently, two replicas were built and are in operation at the Instituto Tecnológico de Aeronáutica (ITA)[2], Brazil, in a cooperative work between U-M and ITA, funded by Financiadora de Estudos e Projetos (FINEP)[3] and EMBRAER[4]. More than 40 flights of the X-HALE were accomplished by the ITA team since July 2017.

[1] https://a2srl.engin.umich.edu/research/flexible/xhale/. Accessed May 2019.
[2] http://www.lnca.ita.br/?q=node/18. Accessed May 2019.
[3] http://www.finep.gov.br/. Accessed May 2019.
[4] https://embraer.com/br/pt. Accessed May 2019.

3.1 Model Description

The mathematical formulation used to model the X-HALE flight dynamics is based on the equations of motion derived for dually-constrained axes [6, 7]. In this formulation, the origin S of the structural axes, corresponding to a material point without elastic displacement, can be non-coincident with the origin O of the body axes used in the equations of motion. In calculating equilibrium conditions, all the structural degrees of freedom are considered. In modeling the nonlinear flight dynamics around equilibrium, a reduced set of inertia-relieved constrained modes of vibration [6, 7] are retained.

The aerodynamic model of the aircraft is based both on the doublet-lattice method [10] and on the vortex-lattice method [11] to which the former reduces at zero frequency. Rational function approximations [6, 12] are used to make the representation of aerodynamic loads possible in the time domain. Consequently, a significant number of aerodynamic lag states arise to make the approximation sufficiently accurate. The induced drag is also modeled, based on the method of Ref. [13].

The wing structural-dynamic model consists of beam finite elements along the span. The beam element formulation is as explained in Refs. [14, 15]. Beam elements are also used for the connection between the wing and the booms and for the booms themselves. The horizontal tails are modeled with rigid elements. Small deformations are assumed.

The vector of state variables for the full-order nonlinear model is given by:

$$\mathbf{X_{full}} = \left[\begin{array}{cccccccccccccccc} V & \alpha & q & \theta & h & x & \beta & \phi & p & r & \psi & y & \boldsymbol{\lambda_{rb}}^T & \boldsymbol{\eta}^T & \dot{\boldsymbol{\eta}}^T & \boldsymbol{\lambda_{\eta}}^T \end{array} \right]^T \tag{9}$$

The model includes the kinematic equations in the inertial reference frame for all six rigid-body degrees of freedom: displacements in the x and y directions, altitude h, and roll, pitch and yaw angles (ϕ, θ and ψ, respectively). Furthermore, the velocity V, the angle of attack α, the sideslip angle β, as well as the angular rates p, q and r also have their corresponding equations of motion. The modal amplitudes and their time derivatives are given by $\boldsymbol{\eta}$ and $\dot{\boldsymbol{\eta}}$, respectively. Modes of vibration with frequencies up to 25 Hz are retained in the model. Aerodynamic lag states due to rigid-body and control-surface dynamics ($\boldsymbol{\lambda_{rb}}$) and due to the aeroelastic dynamics ($\boldsymbol{\lambda_{\eta}}$) are also included.

The full-order model comprises 219 states: 12 (rigid-body motion) $+$ 63 (rigid-body plus control-surface aerodynamic lag states) $+$ 32 (aeroelastic states) $+$ 112 (aeroelastic aerodynamic lag states). Moreover, seven uncorrelated actuators, including two elevons (δ_{le} and δ_{re}), two ailerons (δ_{la} and δ_{ra}) and three electric motors (τ_l, τ_c and τ_r) make up the control inputs of the aircraft (see Fig. 2):

$$\mathbf{U_{full}} = \left[\begin{array}{ccccccc} \delta_{la} & \delta_{le} & \delta_{re} & \delta_{ra} & \tau_l & \tau_c & \tau_r \end{array} \right]^T \tag{10}$$

where the subscript l means left (port) side of the aircraft, r right (starboard) side, and c central position, whereas the subscripts a and e represent the ailerons and elevons, respectively. The δ variables correspond to the control surfaces deflections, given in degrees, and the τ variables correspond to the throttle setting of each motor, varying from zero (no thrust) to one (full throttle).

The output vector $\mathbf{Y_{full}}$ comprises 207 model outputs such as velocity, altitude, angles of attack and sideslip, displacements, elastic rotations, attitude angles, angular velocities, load factors and strain gauge measurements at different points along the wing.

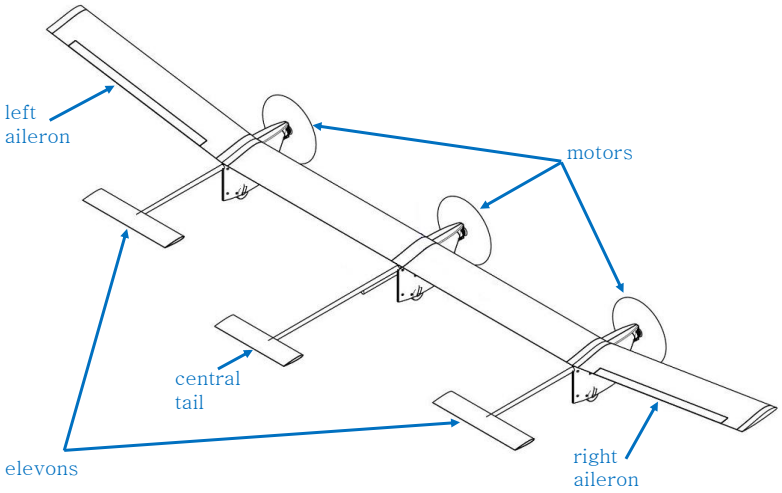

Figure 2: Actuators' description of the four-meter-span, horizontal-central-tail X-HALE configuration.

The measurements made possible by the aircraft sensors ($\mathbf{Y}_{\mathbf{sens}}$) are a subset of the model outputs and contain accelerations, angular rates and attitude angles measured by three Inertial Measurement Units (IMU)/Attitude Heading Reference Systems (AHRS) placed at both wing tips and near the aircraft center of gravity (CG):

$$\mathbf{Y}_{\mathbf{sens}} = \begin{bmatrix} \boldsymbol{a}_l^{xyz} & \boldsymbol{\omega}_l & \boldsymbol{\Phi}_l & \boldsymbol{a}_c^{xyz} & \boldsymbol{\omega}_c & \boldsymbol{\Phi}_c & \boldsymbol{a}_r^{xyz} & \boldsymbol{\omega}_r & \boldsymbol{\Phi}_r \end{bmatrix}^T \tag{11}$$

where $\boldsymbol{a}_\bullet^{xyz} = \begin{bmatrix} a_\bullet^x & a_\bullet^y & a_\bullet^z \end{bmatrix}^T$ comprises the accelerations in the x, y, and z directions of a sensor Cartesian coordinate systems; $\boldsymbol{\omega}_\bullet = \begin{bmatrix} p_\bullet & q_\bullet & r_\bullet \end{bmatrix}^T$ corresponds to the respective angular rates; and $\boldsymbol{\Phi}_\bullet = \begin{bmatrix} \phi_\bullet & \theta_\bullet & \psi_\bullet \end{bmatrix}^T$ contains the sensor attitude angles. The subscript $\bullet$ refers to the IMU/AHRS positions – left (l) and right (r) wing tip and close to CG (c). Details about the current data acquisition system of the ITA's X-HALE can be found in Ref. [16].

In Eqs. (9) and (10), the uppercase letters $\mathbf{X}$ and $\mathbf{U}$ denote the instantaneous values of the states and control inputs in the nonlinear equations of motion. Moreover, for simplicity of notation, their functional dependence on time (t) was suppressed. Both statements are also valid for $\mathbf{Y}_{\mathbf{full}}$ and $\mathbf{Y}_{\mathbf{sens}}$.

3.2 Linearization and Aircraft Command Laws

A linearization of the full-order nonlinear dynamic model is mandatory in the design of the control system addressed in this paper. Therefore, considering the theory of small disturbances around a certain steady-state flight condition, the following linearized dynamics arises [6, 17]:

$$\dot{\mathbf{x}}_{\mathbf{full}} = \mathbf{A}_{\mathbf{full}}\mathbf{x}_{\mathbf{full}} + \mathbf{B}_{\mathbf{full}}\mathbf{u}_{\mathbf{full}} \tag{12}$$

$$\mathbf{y}_{\mathbf{full}} = \mathbf{C}_{\mathbf{full}}\mathbf{x}_{\mathbf{full}} + \mathbf{D}_{\mathbf{full}}\mathbf{u}_{\mathbf{full}} \tag{13}$$

$$\mathbf{y}_{\mathbf{sens}} = \mathbf{C}_{\mathbf{sens}}\mathbf{x}_{\mathbf{full}} \tag{14}$$

where the coefficient matrices $\mathbf{A}_{\mathbf{full}} \in \mathbb{R}^{219\times219}$, $\mathbf{B}_{\mathbf{full}} \in \mathbb{R}^{219\times7}$, $\mathbf{C}_{\mathbf{full}} \in \mathbb{R}^{207\times219}$, $\mathbf{D}_{\mathbf{full}} \in \mathbb{R}^{207\times7}$ and $\mathbf{C}_{\mathbf{sens}} \in \mathbb{R}^{27\times219}$ are Jacobian matrices [17] calculated at the equilibrium point of such flight condition. In Eqs. (12) to (14), the lowercase notation for the state, control and output vectors indicates disturbances around their corresponding equilibrium values. Furthermore, their time dependence is also implicit.

In this work, the linearized model used in control system design is obtained around a straight level flight condition, at an altitude of 650 meters in the International Standard Atmosphere and with velocity of 16 meters per second, which is typically used in the ITA X-HALE flights.

As stated before, all aircraft actuators can be independently controlled. However, to accomplish aircraft control in a more conventional way, pitch attitude is controlled by the elevons δ_{le} and δ_{re} operating symmetrically as elevator ($\delta_e = \delta_{re} = \delta_{le}$); the rolling motion is controlled by the ailerons δ_{la} and δ_{ra} operating anti-symmetrically ($\delta_{ra,antisym} = -\delta_{la,antisym}$, $\delta_a = \left(\delta_{ra,antisym} - \delta_{la,antisym}\right)/2$), whereas the yawing motion is controlled using differential throttle of the external motors ($\tau_c - \tau_l = \tau_r - \tau_c = \tau_{rd}$). The global thrust level of the three motors responds to the throttle command (τ_{th}).

The described mixing of control inputs corresponds to the controls available to the pilot. In addition, the aircraft flight control system (FCS) [16] can add a symmetrical parcel of aileron actuation ($\delta_{ra,sym} = \delta_{la,sym}$, $\delta_{sym} = \left(\delta_{ra,sym} + \delta_{la,sym}\right)/2$) to the pilot commands aiming to regulate the structural shape.

Then, in terms of input vector for the linear model, all defined aircraft command laws can be written as:

$$\mathbf{u} = \begin{bmatrix} \Delta\tau_{th} & \Delta\delta_e & \Delta\delta_a & \Delta\tau_{rd} & \Delta\delta_{sym} \end{bmatrix}^T \tag{15}$$

where $\mathbf{u} \in \mathbb{R}^{5\times 1}$ and $\Delta\tau_{th}$, $\Delta\delta_e$, $\Delta\delta_a$, $\Delta\tau_{rd}$ and $\Delta\delta_{sym}$ correspond, respectively, to the throttle, elevator, aileron, "rudder" and symmetrical aileron disturbances from their respective equilibrium values.

The previous assumptions are mathematically represented by the following restructuring of Eqs. (12) and (13):

$$\mathbf{B}_\delta = \begin{bmatrix} (\mathbf{B_5} + \mathbf{B_6} + \mathbf{B_7}) & (\mathbf{B_2} + \mathbf{B_3}) & (\mathbf{B_4} - \mathbf{B_1}) & (\mathbf{B_7} - \mathbf{B_5}) & (\mathbf{B_4} + \mathbf{B_1}) \end{bmatrix} \tag{16}$$

$$\mathbf{D}_\delta = \begin{bmatrix} (\mathbf{D_5} + \mathbf{D_6} + \mathbf{D_7}) & (\mathbf{D_2} + \mathbf{D_3}) & (\mathbf{D_4} - \mathbf{D_1}) & (\mathbf{D_7} - \mathbf{D_5}) & (\mathbf{D_4} + \mathbf{D_1}) \end{bmatrix} \tag{17}$$

where $\mathbf{B_j}$ represents the j-th column of the matrix $\mathbf{B_{full}}$ and $\mathbf{D_j}$ the j-th column of $\mathbf{D_{full}}$. $\mathbf{B}_\delta \in \mathbb{R}^{219\times 5}$ and $\mathbf{D}_\delta \in \mathbb{R}^{207\times 5}$. Therefore, taking into account the restrictions of the command laws definitions, the aircraft linearized dynamics becomes:

$$\dot{\mathbf{x}}_{\mathbf{full}} = \mathbf{A_{full}}\mathbf{x_{full}} + \mathbf{B}_\delta\mathbf{u} \tag{18}$$

$$\mathbf{y_{full}} = \mathbf{C_{full}}\mathbf{x_{full}} + \mathbf{D}_\delta\mathbf{u} \tag{19}$$

$$\mathbf{y_{sens}} = \mathbf{C_{sens}}\mathbf{x_{full}} \tag{20}$$

Actuator models are also considered, represented by simple lag transfer functions, with time constant of 48 and 150 milliseconds for the control surfaces and electric motors, respectively. The state-space realization for the set of actuators differential equations can be written as:

$$\dot{\mathbf{x}}_{\mathbf{act}} = \mathbf{A_{act}}\mathbf{x_{act}} + \mathbf{B_{act}}\mathbf{u_c} \tag{21}$$

$$\mathbf{u} = \mathbf{C_{act}}\mathbf{x_{act}} \tag{22}$$

where $\mathbf{A_{act}}$, $\mathbf{B_{act}}$ and $\mathbf{C_{act}} \in \mathbb{R}^{5\times 5}$ are diagonal matrices:

$$\mathbf{x_{act}} = \begin{bmatrix} x_{\tau_{th}} & x_{\delta_e} & x_{\delta_a} & x_{\tau_{rd}} & x_{\delta_{sym}} \end{bmatrix}^T \tag{23}$$

is the actuators state vector and:

$$\mathbf{u_c} = \begin{bmatrix} u_{thc} & u_{ec} & u_{ac} & u_{rdc} & u_{symc} \end{bmatrix}^T \tag{24}$$

is the vector of commanded inputs.

From Eqs (18) to (22), the augmented full-order linear model of the four-meter-span, vertical-central-tail X-HALE is given by:

$$\dot{\mathbf{x}}_\mathbf{a} = \mathbf{A_a x_a} + \mathbf{B_a u_c} \tag{25}$$

$$\mathbf{y_{full}} = \mathbf{C_a x_a} \tag{26}$$

$$\mathbf{y_{sens}} = \mathbf{C_{sensa} x_a} \tag{27}$$

where $\mathbf{A_a} \in \mathbb{R}^{224\times224}$, $\mathbf{B_a} \in \mathbb{R}^{224\times5}$, $\mathbf{C_a} \in \mathbb{R}^{207\times224}$ and $\mathbf{C_{sensa}} \in \mathbb{R}^{27\times224}$.

3.3 Model Order Reduction and Scaling

The high order of the X-HALE model given by Eqs. (25) to (27) is a challenge to most control techniques and therefore an order reduction prior to control system design is appropriate. The residualization technique [18] was chosen based on authors such as Waszak and Schmidt [19], Reschke [20] and Guimarães Neto [6] who have already demonstrated the effectiveness of such method in reducing the order of flexible aircraft models and because it performs better to keep low or medium frequency modes and to preserve the steady-state gain of the system [18].

The resulting reduced-order linear model comprises 8 rigid-body states (with x, y, ψ, and h discarded), 12 aeroelastic states (six modal amplitudes and their time derivatives) related to the modes of vibration described in Table 1, and 5 from actuators dynamics, totalizing 25 states. The modes in Table 1 were selected because they are the dominant in the system input-output relation considering the set of aircraft sensors given by Eq. (11).

Table 1: Modes of vibration related to the aeroelastic states retained in the reduced-order linear model.

Mode	Description	f [Hz]
1	1st symmetric wing bending	2.29
6	1st symmetric wing torsion	4.45
7	1st antisymmetric wing bending	5.69
8	2nd symmetric wing bending	7.97
13	coupled, asymmetric in- and out-of-plane wing bending	12.25
14	coupled, asymmetric in- and out-of-plane wing bending	13.43

Another very important problem concerns model scaling. Improperly scaled linear models can make the control law design process an arduous task. Moreover, it can result in inappropriate controllers [18]. The X-HALE model is characterized by dynamic modes with very different frequencies and, for this reason, scaling is recommended.

The scaling process was applied to the reduced-order linear model considering a diagonal transformation matrix whose elements are the inverse of the maximum expected absolute value of each state. These maximum expected values were estimated by analyzing the time responses of the system to coupled step commands applied to the actuators.

The scaled reduced-order linear model can be represented by:

$$\dot{\mathbf{x}} = \mathbf{A}\mathbf{x} + \mathbf{B}\mathbf{u_c} \tag{28}$$

$$\mathbf{y_{full}} = \bar{\mathbf{C}}\mathbf{x} \tag{29}$$

$$\mathbf{y_{sens}} = \mathbf{C}\mathbf{x} \tag{30}$$

where $\mathbf{A} \in \mathbb{R}^{25\times25}$, $\mathbf{B} \in \mathbb{R}^{25\times5}$, $\bar{\mathbf{C}} \in \mathbb{R}^{207\times25}$ and $\mathbf{C} \in \mathbb{R}^{27\times25}$. The state-space realization ($\mathbf{A}$, $\mathbf{B}$, $\mathbf{C}$) from Eqs. (28) and (30) corresponds to the model used in the control system design. This is the reason why the same notation of Eqs. (1) and (2) was employed.

Figure 3 shows the maximum and minimum singular values of the MIMO (multiple-input, multiple-output) transfer function matrix from $\mathbf{u_c}$ to $\mathbf{y_{sens}}$ for both the full-order and the scaled reduced-order models. It is notorious that the scaled reduced-order model preserves sufficient characteristics of the full-order one.

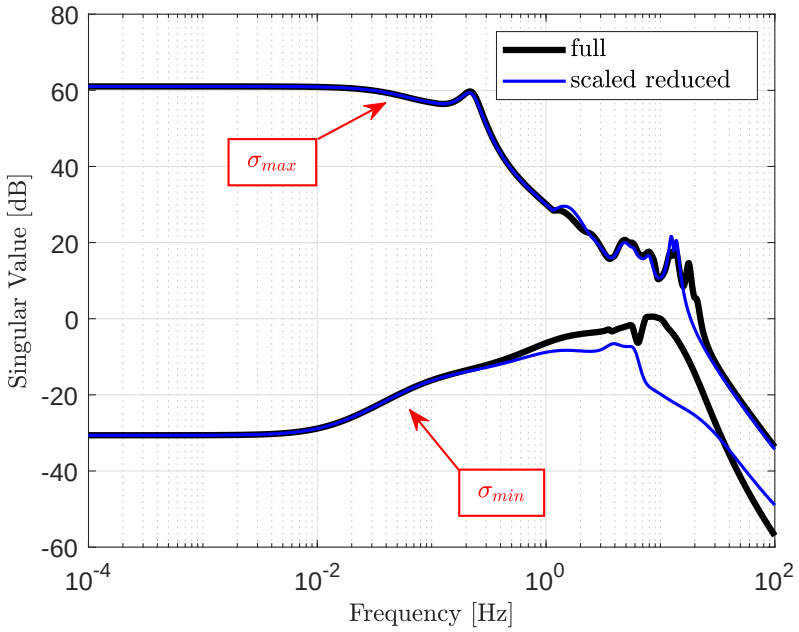

Figure 3: Comparison between the maximum (σ_{max}) and minimum (σ_{min}) singular values of the transfer function matrix ($\mathbf{u_c}$ to $\mathbf{y_{sens}}$) of both full-order and scaled-reduced-order linear models.

4 SAS DESIGN AND ANALYSIS

Using the scaled reduced-order linear model described in the last section, a stability augmentation system (SAS) based on the projective control technique (Eqs. (6) and (7)) was designed and compared with an optimal state feedback one (Eq. (3)). The SAS is an output-feedback-based controller designed to improve both flight and structural dynamics characteristics of the X-HALE.

The design considered the following requirements:

(i) reduction of the spiral (spr) mode time constant ($\tau_{spr} < 2\ s$) and increase of the real-axis coordinate ($\zeta_{dr}\omega_{n_{dr}} > 0.35$) of the dutch-roll (d.r.) mode roots;
(ii) increase of the damping ratio of the first three modes of Table 1 by at least 50%;
(iii) minimal or no degradation of the damping ratio of the other aeroelastic modes.

At this point some aspects deserve attention: firstly, the throttle was not used in the control

system. Then, for simplicity, the following development was performed considering Eqs. (28) and (30) properly truncated to eliminate the state $x_{\tau_{th}}$ and the input u_{thc}.

Second, the requirements for the lateral-directional modes specified in (i) aim both at stability augmentation and at improvement of the handling qualities. The damping ratio (ζ_{dr}) and natural frequency ($\omega_{n_{dr}}$) criteria for the dutch-roll mode follow the military flying-qualities specifications presented in [17]. Although created for manned military aircraft, the specification is a good guideline. Moreover, the authors in [17] suggest that airplanes with large roll-yaw coupling are subject to a more stringent requirement on $\zeta_{dr}\omega_{n_{dr}}$. The spiral mode requirement is just for faster response. The improvement of lateral-directional handling qualities as required would also increase the stability of the horizontal-central-tail configuration of the aircraft, which is not analyzed in this paper.

The structural requirements in (ii) aim to reduce the effects of structural modes on the aircraft response in higher-frequency bands. Roughly, this is an attempt to artificially emulate what would be a rigid-body frequency response of the X-HALE. The 50% higher structural damping criterion was an arbitrary choice since such specification is still an open topic in the scientific community. The reason why only the first three modes have been considered will soon be clear.

Lastly, the third requirement only ensures that higher-frequency modes and other modes that already have good dynamic characteristics, such as the longitudinal ones, are at most slightly affected.

Based on such requirements, the optimum state feedback gain was then designed from Eq. (3), with the appropriate choices for the ARE (Eq. (4)) parameters:

$$\mathbf{Q} = \begin{bmatrix} \mathbf{Q_{rb}} & \mathbf{0_{8\times 6}} & \mathbf{0_{8\times 6}} & \mathbf{0_{8\times 4}} \\ \mathbf{0_{6\times 8}} & \mathbf{Q}_\eta & \mathbf{0_{6\times 6}} & \mathbf{0_{6\times 4}} \\ \mathbf{0_{6\times 8}} & \mathbf{0_{6\times 6}} & 2\mathbf{Q}_\eta & \mathbf{0_{6\times 4}} \\ \mathbf{0_{4\times 8}} & \mathbf{0_{4\times 6}} & \mathbf{0_{4\times 6}} & \mathbf{Q_{x_{act}}} \end{bmatrix} \tag{31}$$

$$\mathbf{R} = diag\left(1,\ 1,\ 1/(0.15)^2,\ 1\right) \tag{32}$$

where $diag\,(\bullet)$ represents a diagonal matrix for which the main diagonal elements are given by $\bullet$, and:

$$\mathbf{Q_{rb}} = diag\,(0,\ 0,\ 0,\ 0,\ 1,\ 0.5,\ 0.5,\ 1) \tag{33}$$

$$\mathbf{Q}_\eta = diag\,(0.8,\ 0.4,\ 0.4,\ 0,\ 0,\ 0) \tag{34}$$

$$\mathbf{Q_{x_{act}}} = diag\,(0,\ 0,\ 0.25,\ 0) \tag{35}$$

correspond to the weighting elements of the rigid-body ($\mathbf{Q_{rb}}$), aeroelastic ($\mathbf{Q}_\eta$) and actuator ($\mathbf{Q_{x_{act}}}$) states. The elements of $\mathbf{R}$ were chosen based on Bryson's rule [17]. Table 2 and the pole maps of Fig. 4 show the state feedback design results and compare them with the open-loop system.

The state feedback design meets almost all the requirements: the time constant of spr dropped from 3.03 seconds to 1.18; $\zeta_{dr}\omega_{n_{dr}}$ increased considerably; the damping ratio of the 6th and 7th aeroelastic modes increased by 50% and the 8th, 13th and 14th modes were not affected.

It is noticed, however, that the longitudinal dynamic modes moved to the left, the short period (s.p.) more sharply than phugoid (ph), and that the damping ratio of 1st mode almost did not

Table 2: Open- and closed-loop dynamic characteristics of the modes specified in the design requirements.

Mode	Open Loop	State Feedback
spr	$\tau_{spr} = 3.03\ s$	$\tau_{spr} = 1.18\ s$
d.r.	$\zeta_{dr}\omega_{n_{dr}} = 0.275$	$\zeta_{dr}\omega_{n_{dr}} = 0.766$
1	$\zeta_1 = 0.327$	$\zeta_1 = 0.377$
6	$\zeta_6 = 0.180$	$\zeta_6 = 0.269$
7	$\zeta_7 = 0.151$	$\zeta_7 = 0.236$

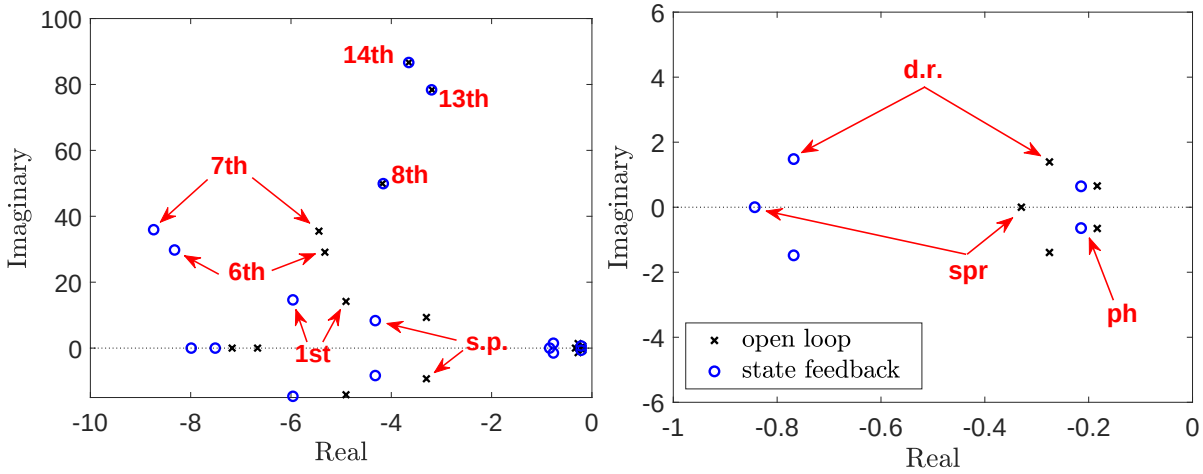

Figure 4: Pole maps comparing the dynamic modes in the open- and closed-loop (state feedback) systems.

change. The former is due to the use of symmetrical aileron and elevator deflections in the feedback. The latter is still not very clear. Moreover, a strong coupling between the s.p. and 1st modes was observed and the results shown correspond thus far to the best trade-off between increasing the damping of the 1st mode and keeping the open-loop s.p. poles.

The poles chosen to be placed using projective control were those of the lateral-directional modes (roll subsidence, spr and d.r.), the 1st, 6th and 7th aeroelastic modes and the s.p. These choices stem from the design requirements, with the exception of the s.p. that was included due to its coupling with the 1st mode.

According to Section 2, twelve outputs available for feedback are necessary for the pole placement, since two of the chosen poles are real (spr and roll subsidence) and the other five are complex conjugate pairs. The selection of such outputs is a point that deserves attention.

For the success of a projective controller, the system must be observable, which makes such control technique very sensor dependent. In fact, throughout the design process, it was noticed that the inadequate choice of the measured signals implied either in excessive control energy or even in the instability of some unassigned modes.

This partly explains why only the first three aeroelastic modes were considered in the design. With the sensors currently available in the aircraft (Eq. (11)), it is not possible to observe the higher-frequency structural modes with more complex mode shapes. The other important reason is that the actuators would not be able to operate in such a frequency range. The limited number of control surfaces would also become a problem.

With the foregoing considerations in mind, the following set of signals was employed in the

output feedback:

$$\mathbf{y_{feedback}} = \begin{bmatrix} \alpha \\ q_c \\ \beta \\ \phi_c \\ p_c \\ r_c \\ a_l^z + a_r^z - 2a_c^z \\ -p_l + p_r \\ \theta_l + \theta_r - 2\theta_c \\ q_l + q_r - 2q_c \\ -a_l^z + a_r^z \\ p_l + p_r - 2p_c \end{bmatrix} \tag{36}$$

With exception of α and β, the other elements of $\mathbf{y_{feedback}}$ correspond either to an element of or to a linear combination of elements of $\mathbf{y_{sens}}$ (described in Eq. (11)). Although not currently available in the aircraft, α and β were considered because they will be in a near future.

The rationale for the selection of outputs in Eq. (36) is as follows: α and q_c were considered due to the s.p. mode; β, ϕ_c, p_c and r_c due to the lateral-directional modes; the 7th and 8th elements of $\mathbf{y_{feedback}}$ correspond to a combination of signals significantly affected by the 1st aeroelastic mode, whereas the 9th and 10th elements are affected by the 6th aeroelastic mode, and, lastly, the 11th and 12th elements are affected by the 7th aeroelastic mode.

Based on Eq. (36), knowing the eigenvectors related to the modes to be assigned in the output feedback and the optimal state feedback gain, the projective controller was designed using Eq. (7). Figure 5 shows the projective control results compared with the state feedback approach. An accurate placement of the poles related to the modes of interest can be seen, whereas the other modes undergo small changes, as desired. Therefore, the controller fulfills the requirements.

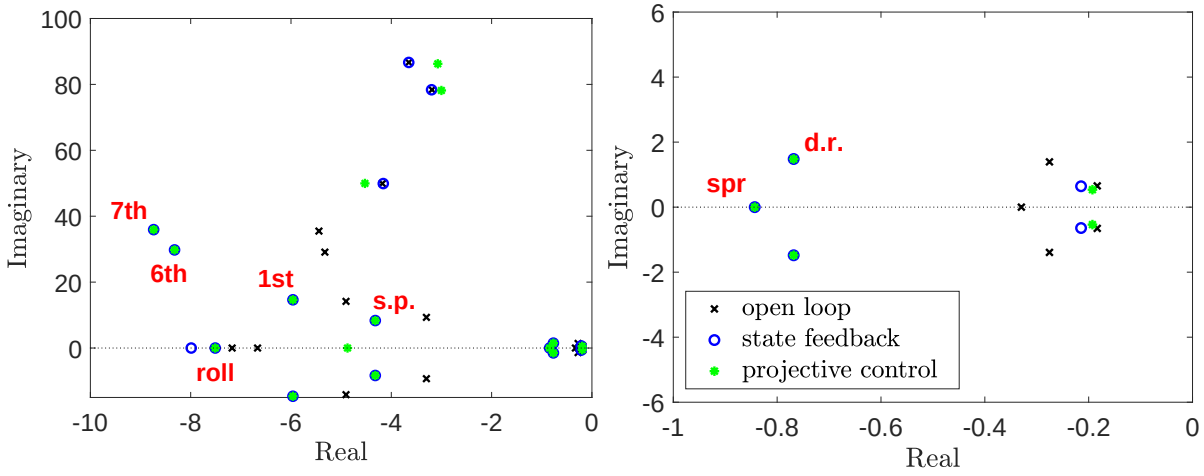

Figure 5: Pole maps comparing the dynamic modes in the open- and closed-loop systems, the latter based either on state feedback or on projective control.

The robustness cited in the objective of this paper corresponds to the attempt to recover the frequency response characteristics of the state feedback approach, since it is well known in the literature [18] that a system with an LQR controller assuming all states are available and no stochastic inputs will have at least 6 dB of lower gain margin and 60° of phase margin.

5 SIMULATION RESULTS

5.1 Aileron Pulse Response

To test the effectiveness of the designed SAS in improving the flight dynamics response, the aircraft was subjected to a positive pulse of 5 degrees applied to the ailerons (δ_a) for 5 seconds. This kind of control input is known to result in strong adverse yaw in the real aircraft, making the use of differential throttle indispensable for coordinating turns. The adverse yaw is caused dominantly by the yawing moment coefficient derivative due to roll rate (C_{n_p}) in such a high-aspect-ratio wing ($AR = 20$), and the simulation model is able to capture it accurately. The results of nonlinear simulations are presented in Figs. 6 to 8, where time histories are shown for the open-loop, the state-feedback, and the projective-control cases.

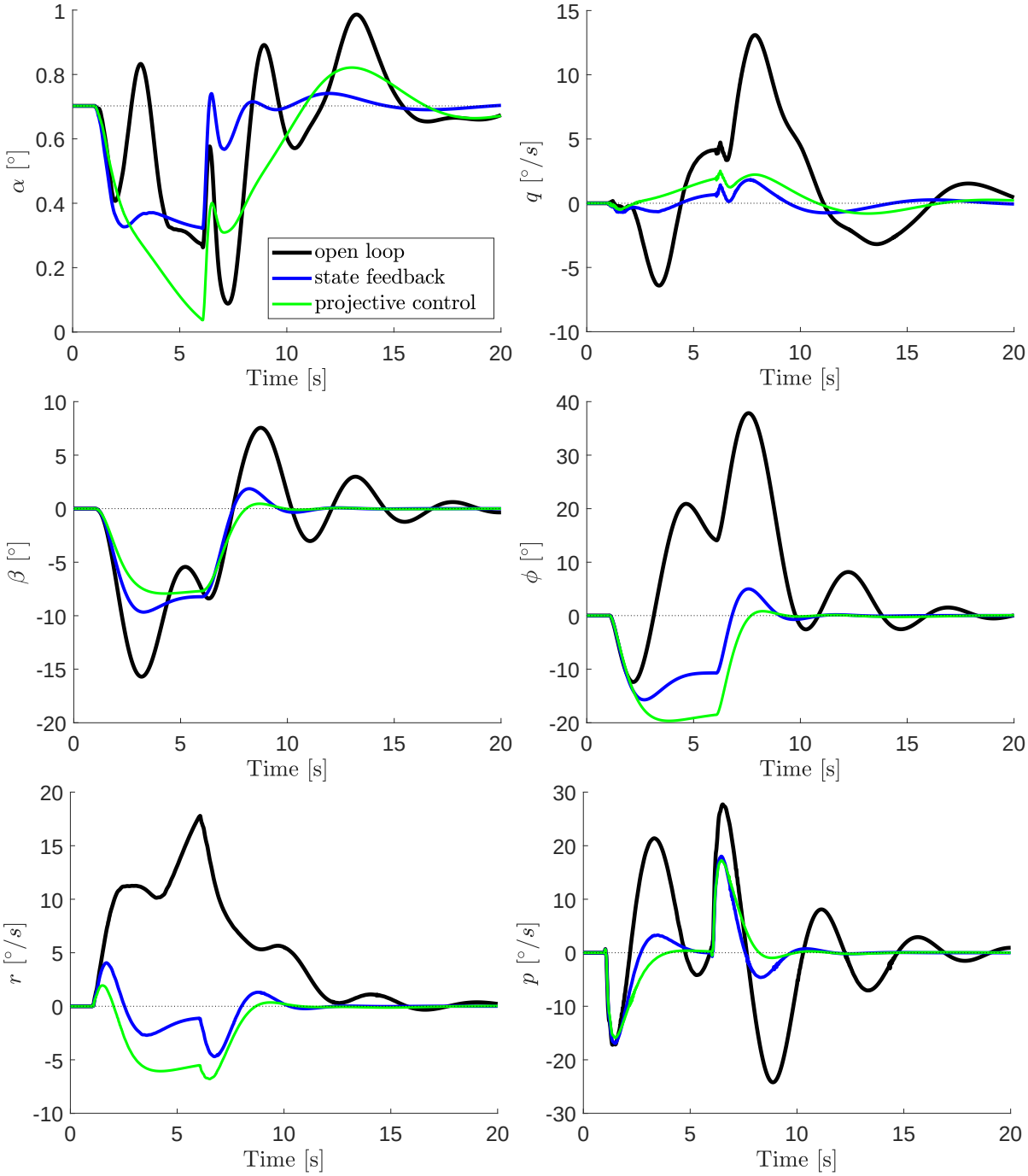

Figure 6: Response to a positive pulse of 5 degrees applied to δ_a: rigid-body states.

The simulation starts with the aircraft in a trimmed straight and level flight condition, kept until $t = 1$ s, when the aileron pulse is applied (Fig. 8). In the open-loop case, Fig. 6 shows that the adverse yaw ($r > 0$) occurs throughout the maneuver. The adverse yaw is so severe that, approximately 1 second after the aileron pulse began, the aircraft begins to roll to the right ($p > 0$). Meanwhile, high absolute values of sideslip angle are attained. The open-loop response would be potentially dangerous in flight, and highly objectionable to the pilot.

Figure 6 also shows that the output-feedback projective controller significantly improves the aircraft lateral-directional response, with performance not much worse than that which would be obtained with state feedback. The adverse yaw is much less intense, now concentrated in the initial second of the maneuver, and caused by the yawing moment produced directly by the aileron deflection. The aircraft in closed loop is able to turn to the left and to sustain negative bank angles with the aileron deflection commanded by the pilot. Fig. 8 shows that the SAS automatically uses the differential throttle to accomplish this.

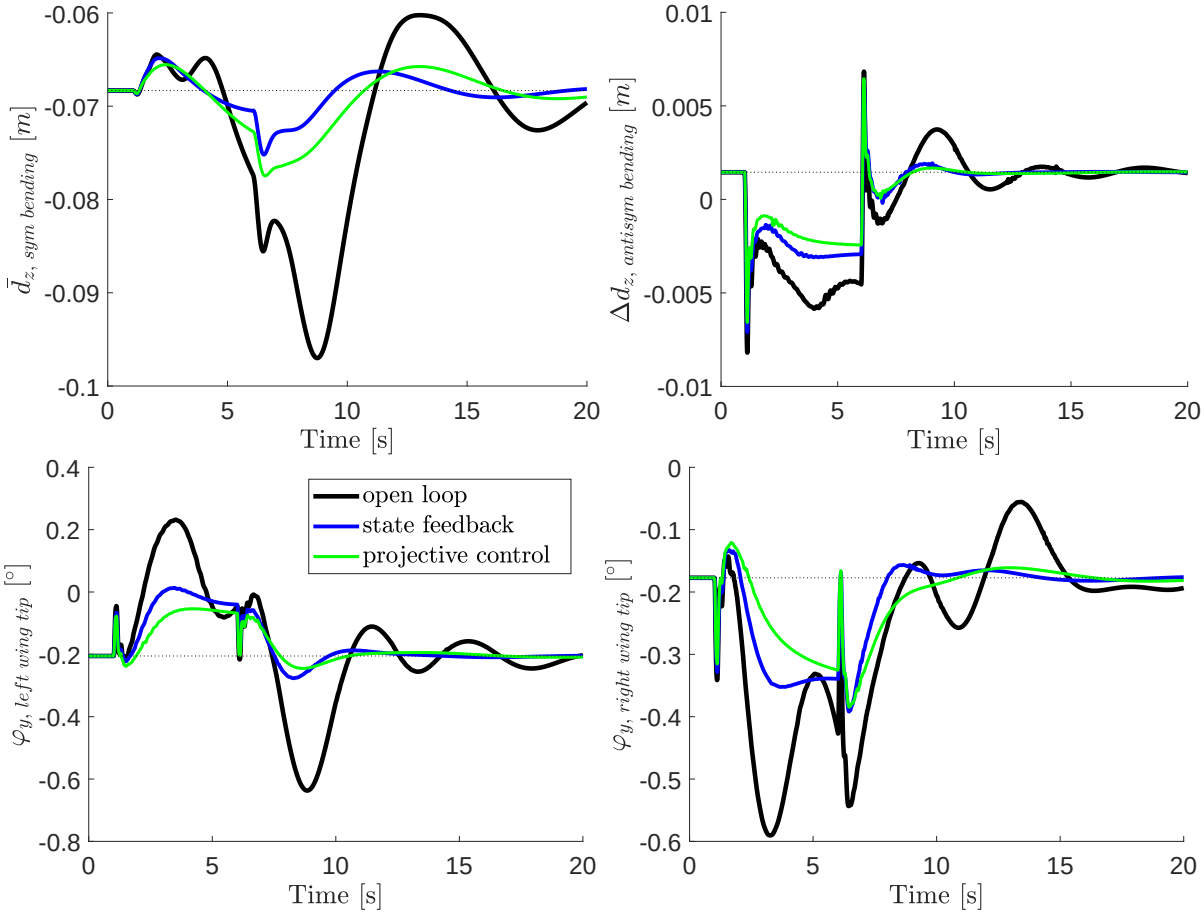

Figure 7: Response to a positive pulse of 5 degrees applied to δ_a: wing tip symmetrical ($\bar{d}_z$) and antisymmetrical (Δd_z) displacements and elastic twist angles (φ_y).

Figure 7 shows the wing tip symmetrical ($\bar{d}_z = (d_{z,\ left\ wing\ tip} + d_{z,\ right\ wing\ tip})/2$) and antisymmetrical ($\Delta d_z = (-d_{z,\ left\ wing\ tip} + d_{z,\ right\ wing\ tip})/2$) displacements and elastic twist angles (φ_y). In this maneuver, the wing deformation is closely related to the rigid-body response. Particularly, Fig. 6 showed that the pitch rate was excited in the open-loop case, and the pitch rate time history is clearly seen to be related to the wing tip symmetrical displacement in Fig. 7. The antisymmetrical bending has small amplitude, and is dominantly caused by aileron deflection. Antisymmetrical torsion is caused by the same effect, but no mode related

to this kind of torsion has been assigned in the design. Because the SAS works very well in improving the lateral-directional response, the structural deformation is also attenuated in the case of the aileron pulse.

Finally, Fig. 8 shows the actuator time histories. All control signals are feasible, that is, they operate with magnitudes and rates smaller than their limits. Very little symmetrical aileron deflection was needed in this maneuver.

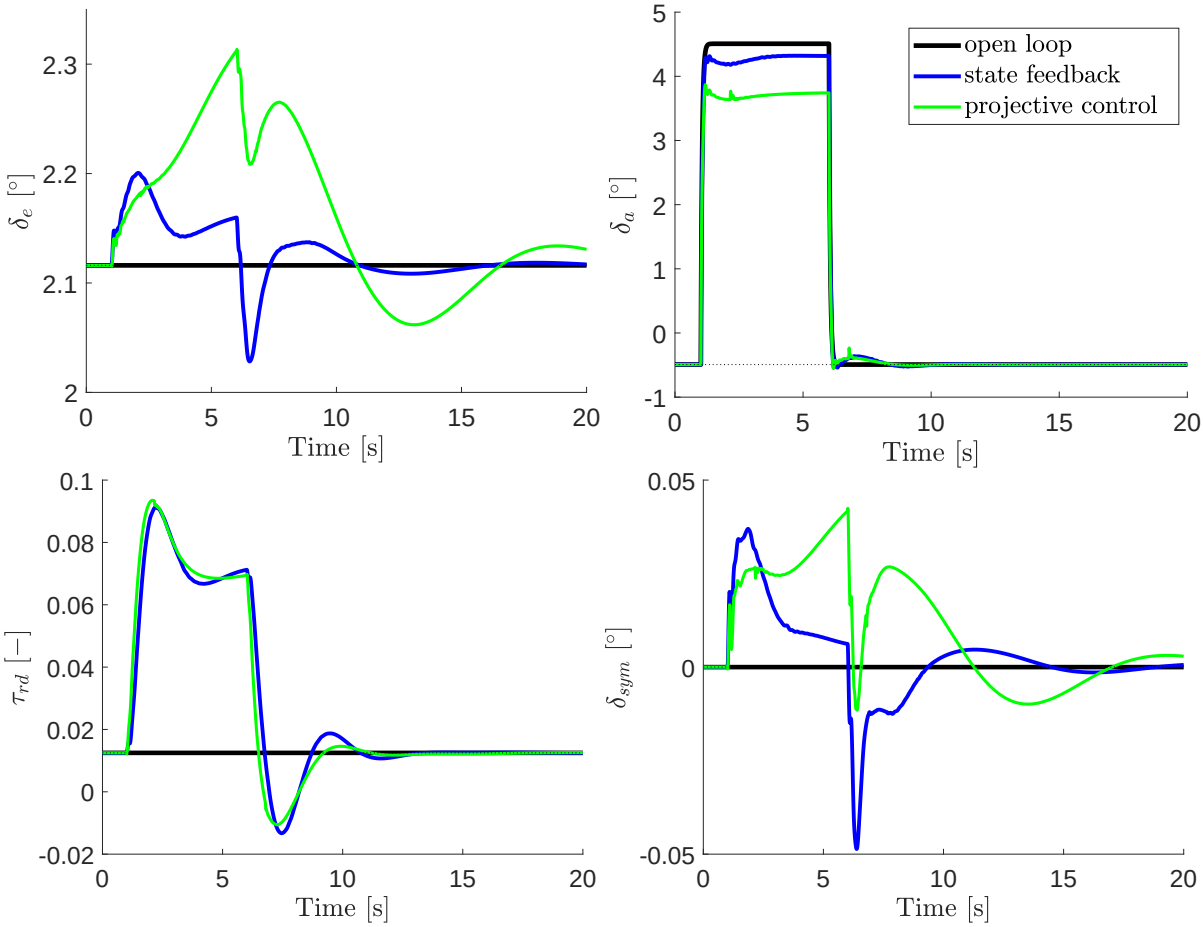

Figure 8: Response to a positive pulse of 5 degrees applied to δ_a: actuator time histories.

5.2 Sinusoidal Vertical Gust Response

To test the effectiveness of the designed SAS in attenuating the structural response, the aircraft was subjected to a theoretical sinusoidal vertical gust in nonlinear simulations. The sinusoidal gust consists of a series of vertical one-minus-cosine gusts, but defined with respect to time t instead of with respect to e.g. the coordinate x. Consequently, the entire aircraft is subjected to the same gust velocity at any instant. The vertical gust velocity profile is given by:

$$V_{g,z,i} = -\frac{w_g}{2}\left(1 - \cos\left(2\pi f_g t\right)\right) \tag{37}$$

for every $t \geq 0$. In Eq. (37), $w_g = 2$ m/s is the maximum gust velocity; the gust frequency $f_g = 2.5$ Hz is tuned to be close to that of the first aeroelastic mode of the aircraft flying at 16 m/s; and the negative sign is due to the facts that $V_{g,z,i}$ is the vertical gust velocity in the inertial reference frame and that an upward gust is considered.

The aerodynamic effects of the gust are included in the form of an additional normalwash in each box of the aircraft vortex-lattice-method model. Hence, flow unsteadiness is not considered

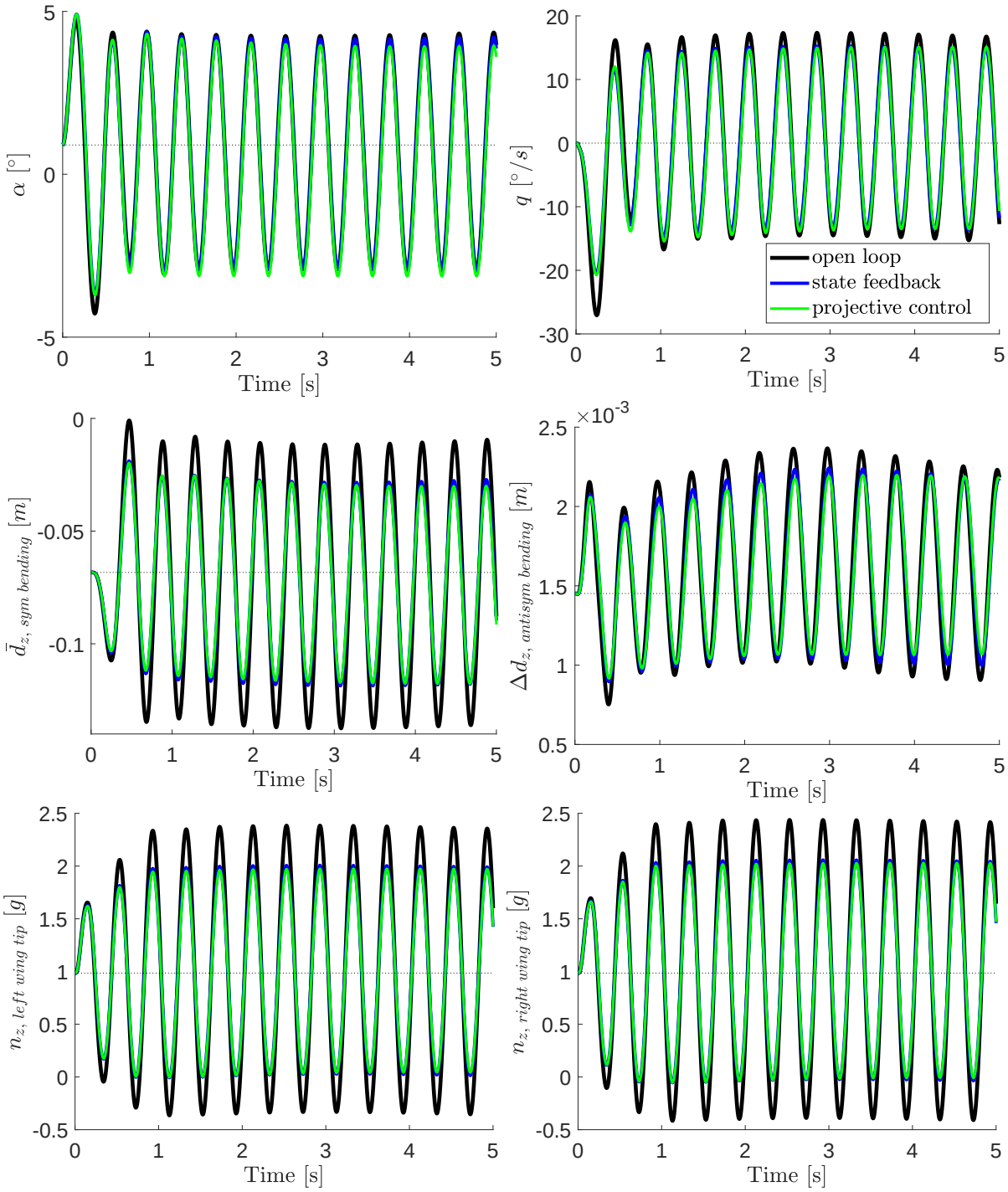

Figure 9: Response to sinusoidal gust: angle of attack, pitch rate, wing tip symmetrical ($\bar{d}_z$) and antisymmetrical (Δd_z) displacements and wing tip normal load factors.

in the interaction between the aircraft and the gust, and this simplifying assumption is consistent with the consideration of no gust penetration effect in Eq. (37).

The results of nonlinear simulations of the aircraft response to five seconds of sinusoidal vertical gust are presented in Figs. 9 and 10, where time histories are shown for the open-loop, the state-feedback, and the projective-control cases.

The wing tip symmetrical displacements ($\bar{d}_z$) had their amplitudes reduced from approximately $6\ cm$ (open loop) to $4.3\ cm$ (both closed-loop cases). Similar attenuation levels can be seen for

the normal load factors that would be measured by accelerometers installed at the wing tips, for which the closed-loop responses in both cases presented attenuation of approximately 33%.

Once more all control signals are feasible, operating within their magnitude and rate limits, as seen in Fig. 10. As expected, the symmetrical aileron deflection is the dominant control in this case, since the sinusoidal gust was tuned to be close to the frequency of the first wing symmetric bending aeroelastic mode. Elevator deflection is also present and is related to the slight attenuation of the angle of attack and pitch rate time histories in Fig. 9.

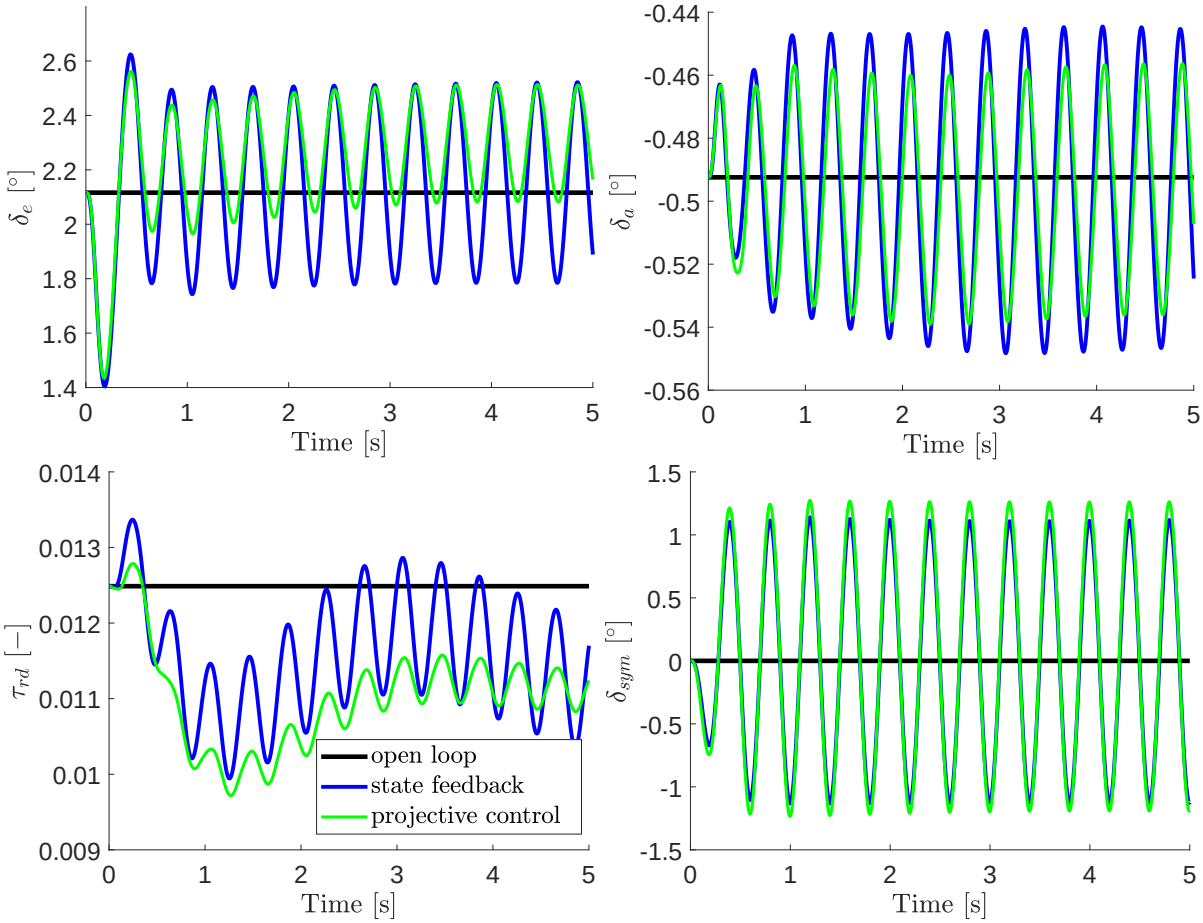

Figure 10: Response to sinusoidal gust: actuator time histories.

6 CONCLUSIONS

In this paper a stability augmentation system based on the projective control technique was developed and applied to the X-HALE flexible aircraft. This output feedback control technique allows preserving in the closed-loop system the eigenstructure of certain modes of interest whose dynamic characteristics stem from an optimal state feedback solution.

The use of the projective control technique, together with a dynamic formulation that captures the aircraft aeroelastic response, was seen to be promising and advantageous in dealing with the challenges of flexible aircraft control. It is promising because it allows to easily incorporate frequency and damping specifications that are particularly important when dealing with aeroelastic modes. And it is advantageous because, from the point of view of practical implementation, the design is straightforward and the resulting controller is of low order.

Nonlinear simulation results showed the effectiveness of the designed stability augmentation

system in drastically improving the lateral-directional handling qualities and in attenuating the aircraft aeroelastic response. With the aircraft excited by an aileron pulse lasting five seconds, the projective controller was able to avoid potentially dangerous phenomena related to the adverse yaw and the strong roll-yaw coupling of the high-aspect-ratio wing. In the response to a theoretical sinusoidal vertical gust, tuned at a frequency close to that of the first aeroelastic, symmetric wing bending mode, the controller was able to attenuate wing tip displacements and load factors. In general, the projective control performance was very similar to that of the optimal state feedback.

A characteristic of the proposed control system design methodology is the need for as many outputs for feedback as there are poles to be assigned. Particularly, in the four-meter-span configuration of the X-HALE analyzed in this paper, the number of sensors is limited, as only sensors located at the wing tips or near the wing central station are available. Hence, this is a limitation on the number and the shapes of modes that can be assigned in the control system design. Moreover, one cannot forget that the number, location and dynamic characteristics of actuators are also important for the controllability of higher-frequency modes.

7 ACKNOWLEDGMENT

This work has been supported in part by FINEP and EMBRAER under the research project Advanced Studies in Flight Physics, contract number 01.14.0185.00.

8 REFERENCES

[1] Gadient, R., Lavretsky, E., and Wise, K. (2012). Very flexible aircraft control challenge problem. In *AIAA Guidance, Navigation, and Control Conference*. p. 4973.

[2] Kubica, F. and Livet, T. (1994). Flight control law synthesis for a flexible aircraft. In *AIAA Guidance, Navigation, and Control Conference*. p. 3630.

[3] Silvestre, F. J., Guimarães Neto, A. B., Bertolin, R. M., da Silva, R. G. A., and Paglione, P. (2016). Aircraft control based on flexible aircraft dynamics. *Journal of Aircraft*, 54(1), 262–271.

[4] Lavretsky, E. and Wise, K. (2013). Robust and adaptive control. In *Advanced Textbooks in Control and Signal Processing*. Springer.

[5] Tharp, H. S., Medanic, J. V., and Perkins, W. R. (1986). Robust projective controls for structured perturbations. In *American Control Conference*. IEEE, pp. 1833–1838.

[6] Guimarães Neto, A. B. (2014). *Flight dynamics of flexible aircraft using general body axes: a theoretical and computational study*. Ph.D. thesis, Instituto Tecnológico de Aeronáutica.

[7] Guimarães Neto, A. B., da Silva, R. G. A., Paglione, P., and Silvestre, F. J. (2016). Formulation of the flight dynamics of flexible aircraft using general body axes. *AIAA Journal*, 54(11), 3516–3534.

[8] Cesnik, C. E. S., Senatore, P. J., Su, W., Atkins, E. M., and Shearer, C. M. (2012). X-HALE: A very flexible unmanned aerial vehicle for nonlinear aeroelastic tests. *AIAA journal*, 50(12), 2820–2833.

[9] Anderson, B. D. O. and Moore, J. B. (2007). *Optimal control: linear quadratic methods*. Courier Corporation.

[10] Albano, E. and Rodden, W. P. (1969). A doublet-lattice method for calculating lift distributions on oscillating surfaces in subsonic flows. *AIAA Journal*, 7(2), 279–285. doi: 10.2514/3.5086.

[11] Hedman, S. G. (1965). Vortex lattice method for calculation of quasi steady state loadings on thin elastic wings. Tech. Rep. 105, Aeronautical Research Institute of Sweden, Stockholm.

[12] Eversman, W. and Tewari, A. (1991). Consistent rational function approximation for unsteady aerodynamics. *Journal of Aircraft*, 29(9), 545–552. doi:10.2514/3.46062.

[13] Kálmán, T. P., Giesing, J. P., and Rodden, W. P. (1970). Spanwise distribution of induced drag in subsonic flow by the vortex lattice method. *Journal of Aircraft*, 7(6), 574–576. doi:10.2514/3.44219.

[14] Guimarães Neto, A. B., Silvestre, F. J., Cardoso-Ribeiro, F. L., Bussamra, F. L. S., Silva, R. G. A., and Cesnik, C. E. S. (2017). Validity of the assumption of small deformations in aircraft with different levels of structural flexibility. In *International Forum on Aeroelasticity and Structural Dynamics (IFASD) 2017*. Como, Italy. IFASD-2017-080.

[15] Guimarães Neto, A. B., Cardoso-Ribeiro, F. L., and Silvestre, F. J. (2018). Applicability of geometrically-linear structural-dynamic models for the flight dynamics of arbitrarily-flexible aircraft. In *31st Congress of the International Council of the Aeronautical Sciences (ICAS) 2018*. Belo Horizonte, Brazil. ICAS2018-0523.

[16] Barbosa, G. C., Bertolin, R. M., Paulino, J. A., Silvestre, F., and Guimarães Neto, A. B. (2019). Design and flight test of a stability augmentation system for a flexible aircraft. In *AIAA Scitech 2019 Forum*. p. 0365.

[17] Stevens, B. L., Lewis, F. L., and Johnson, E. N. (2015). *Aircraft control and simulation: dynamics, controls design, and autonomous systems*. India: John Wiley & Sons.

[18] Skogestad, S. and Postlethwaite, I. (2007). *Multivariable feedback control: analysis and design*, vol. 2. India: Wiley India.

[19] Waszak, M. R. and Schmidt, D. K. (1988). Flight dynamics of aeroelastic vehicles. *Journal of Aircraft*, 25(6), 563–571.

[20] Reschke, C. (2006). *Integrated flight loads modelling and analysis for flexible transport aircraft.* Ph.D. thesis, Institut Flugmechanik und Flugregelung der Universitat Stuttgart, Stuttgart.

COPYRIGHT STATEMENT